ARMA 12-493

Perforation of rockfall protection barriers by normal block impact

Hambleton, J.P, Buzzi, O., Giacomini, A., Spadari, M., and Sloan, S.W.
Centre for Geotechnical and Materials Modelling, The University of Newcastle, Callaghan, NSW, Australia

Copyright 2012 ARMA, American Rock Mechanics Association

This paper was prepared for presentation at the 46th US Rock Mechanics / Geomechanics Symposium held in Chicago, IL, USA, 24-27 June 2012.

This paper was selected for presentation at the symposium by an ARMA Technical Program Committee based on a technical and critical review of the paper by a minimum of two technical reviewers. The material, as presented, does not necessarily reflect any position of ARMA, its officers, or members. Electronic reproduction, distribution, or storage of any part of this paper for commercial purposes without the written consent of ARMA is prohibited. Permission to reproduce in print is restricted to an abstract of not more than 300 words; illustrations may not be copied. The abstract must contain conspicuous acknowledgement of where and by whom the paper was presented.

ABSTRACT: Flexible rockfall protection barriers are used ubiquitously to safeguard people and infrastructure against falling rock fragments along weak or fractured slopes. Performance of these barriers is often quantified in terms of the level of impact (kinetic) energy that can be withstood, referred to here as the "critical energy." As pointed out in recent papers, however, there is no single representative value of critical energy for a given barrier. Instead, critical energy decreases as the block size decreases, a phenomenon referred to as the "bullet effect." With a view towards explaining and predicting the bullet effect, the paper presents a simple analytical model for perforation of a flexible barrier caused by normal impact. The model rests on a two-dimensional idealization of the full three-dimensional impact problem, as well as a balance of energy between the initial kinetic energy of the block and the energy absorbed by the barrier. The model predicts a strong dependence of the critical energy on the block size, and the predicted trend agrees well with data available in the literature. Ramifications for practical applications and possible future refinements to the model are also discussed.

1. INTRODUCTION

Rockfall protection barriers are engineered devices installed in strategic locations to intercept blocks of rock along unstable slopes, thereby preventing possible human casualties and damage to sensitive infrastructure. Among all possible forms of rockfall protection (shelters, earth dams, etc.), flexible barriers are popular for their combined versatility and effectiveness at arresting blocks over a relatively broad spectrum of sizes and velocities. A standard flexible barrier, shown schematically in Fig. 1, consists of a wire mesh supported by a system of cables and posts anchored to the rock face or concrete foundations.

Design of a flexible barrier is accomplished in two distinct phases. In the first phase, the possible ranges of block sizes and velocities are identified, with the latter usually determined from numerical simulations of rockfall trajectories. In the second phase, the dimensions and materials for the barrier are selected so that the barrier can withstand worst-case impacts. Naturally, the severity of the impact increases as either block size or velocity increases, and it is therefore common practice to express a barrier's performance in terms of the impact energy, which generally consists of both translational and rotational kinetic energy. The basic determinant of a given barrier's functionality is thus the threshold of impact energy at which blocks will break through the barrier, i.e., the "critical energy." In this paper, critical energy is denoted by E_k.

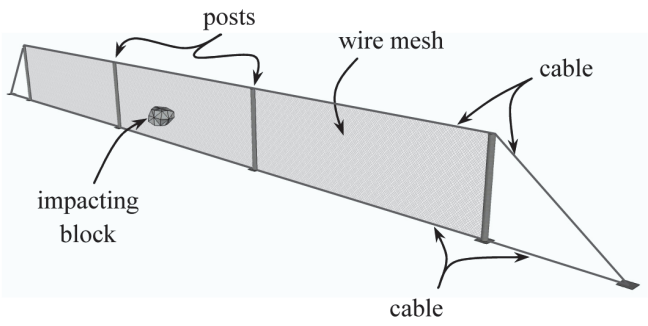

Fig. 1. Schematic of a flexible rockfall protection barrier.

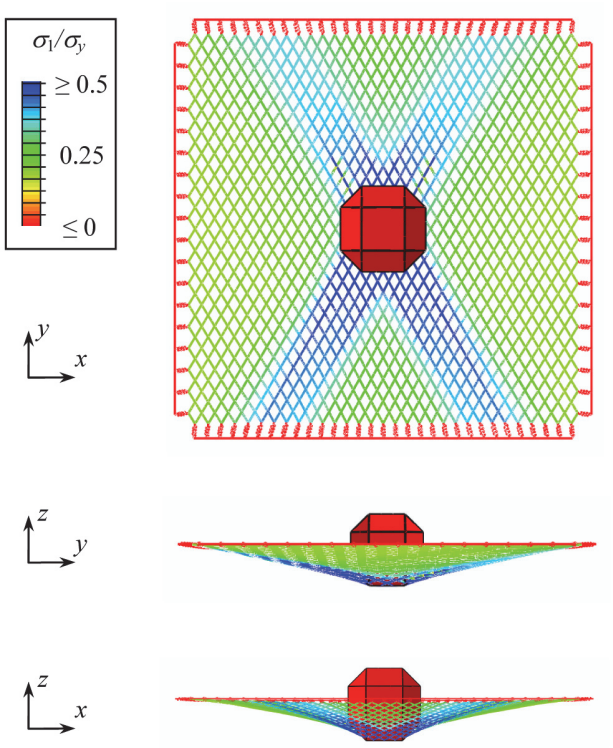

Fig. 2. Deformed configuration from numerical simulation of block impact on a wire mesh supported by springs. Contours show axial stress in the wires (σ_1) normalized by yield strength (σ_y). At the instant shown, the block moves into the mesh with some velocity, and perforation has not yet occurred.

The critical energy E_k for a flexible barrier is most reliably determined by physical tests (e.g., [1-6]), however large costs and long set-up times have motivated a number studies in which block impact on a barrier is simulated numerically (e.g., [7-11]). In both experiments and simulations, it has been observed that there is no single value of E_k for a barrier but rather a range of critical energies for different block sizes. In particular, critical energy decreases as the nominal block diameter, D_b, decreases [8-14]. This apparent decrease in barrier performance with block size is referred to as the "bullet effect," and its implications can be significant. For example, numerical simulations by Cazzani et al. [8] of a full barrier (30 m × 3 m) indicate that the critical energy can drop as much as an order of magnitude as the block diameter is reduced from 1.3 m to 0.3 m. In practical terms, the bullet effect requires that physical tests or numerical simulations must be conducted for an array of block sizes, which comes at potentially great cost or computational expense. Analytical models characterizing this effect are therefore highly desirable. To the authors' knowledge, none have been attempted.

As a means of explaining and predicting the bullet effect, this paper presents a simple analytical model for perforation of a flexible rockfall protection barrier by block impact. As in a recent study by several of authors [15], it is assumed that the block impacts centrally and normally on the wire mesh, and rather than incorporate details of the full barrier in the model, the barrier is represented by a rectangular section of wire mesh supported on its perimeter by springs of an effective stiffness (or flexibility). The flexibility of these springs is selected so as to match the compliance of the structural elements of the barrier (cables, posts, anchors, etc.).

To introduce relevant variables for the problem and motivate the assumptions of the proposed analytical model, the next section describes the typical three-dimensional deformation observed from numerical simulations [15]. In Section 3, the analytical model is formulated by considering a two-dimensional idealization of the problem and a balance of energy between the initial kinetic energy of the block and the energy absorbed by the barrier. In the penultimate section, the predicted dependence of critical energy on block size is compared with results available in the literature.

2. 3D BLOCK IMPACT

Figure 2 shows a typical pattern of deformation and axial stresses in the wire mesh as observed in a finite element simulation of block impact, where the simulation was performed as described by Spadari et al. [15] using ABAQUS/Explicit. The block has a shape taken as the one suggested by EOTA testing guidelines [16], and it impacts with a specified initial normal velocity at the center of a rectangular section of chain link mesh (diamond-shaped pattern) supported at its edges by springs of stiffness K. The block behaves as an elastic solid (Young's modulus of 30 GPa and Poisson's ratio of 0.3), and the wire mesh is composed of rigidly connected beam elements of circular cross section with fixed elastic properties (Young's modulus of 210 GPa and Poisson's ratio of 0.3) but variable yield strength, σ_y, and diameter, D_w. The density of the block, ρ, is 2400 kg/m^3, and the density of the wire is 7800 kg/m^3. For the wire, the plastic strain corresponding to failure is set to 10%. Upon reaching this strain limit, corresponding elements are deleted from the model (i.e. the mesh is perforated). For a given configuration, the value of initial velocity required to perforate the mesh, or the "critical velocity," denoted by v, was determined iteratively by adjusting the initial velocity of the block until perforation of the mesh occurred. Further details regarding the finite element simulations can be found in previous papers by several of the authors [11, 15].

Figure 2 reveals a cross-shaped distribution of axial stresses in which the largest stresses are transmitted in the direction of the nearest support along stands of the

mesh in contact with the block. This pattern was characteristic of all simulations performed, and it was also observed in previous numerical simulations conducted by Anderheggen et al. [7]. In terms of the deformation, the wires are stretched much more in the *y*-direction than the *x*-direction, as manifested through lower curvature of the mesh in the *y*-*z* plane as compared to the *x*-*z* plane.

On account of the observations above, it is reasonable to expect that the full system of wires and springs from Fig. 2 should behave in a manner similar to the system shown in Fig. 3, where regions of mesh with low axial stress have been removed. This reduced system consists of two intersecting strips of mesh, where each strip has an "effective width" denoted by L_e. In light of the pattern shown in Fig. 2, and for the sake of simplicity, L_e is estimated as $L_e \approx D_b$. By further assuming that the two strips behave independently and ignoring variations across the width of the strips, it follows that calculations can be performed on a unit-width basis. Thus, the three-dimensional problem can be conceptually reduced to the two-dimensional analogue shown in Fig. 4. In the next section, this two-dimensional counterpart of the full impact problem is used to obtain analytical predictions of critical energy E_k and critical velocity v.

3. 2D MODEL

For the simple two-dimensional problem shown in Fig. 4, it is a straightforward to compute the energy absorbed by the barrier at incipient failure of the mesh. Through conservation of energy, this absorbed energy is precisely equal to the critical kinetic energy of the block E_k. In this paper, the energy absorbed by the wire mesh itself is neglected, and the impact energy is taken to be absorbed only by the springs that support the mesh along its perimeter. While this may seem unrealistic, the stiffness of these springs is usually relatively low when calibrated to represent a full barrier (cf. [15]), and the springs are indeed the main source of energy absorption. The absorbed energy per unit length of the mesh at failure, denoted by E_f, is thus simply

$$E_f = \frac{1}{2}\left(\frac{K_l}{2}\right)e_f^2 = \frac{F_f^2}{K_l} \tag{1}$$

where K_l is spring stiffness per unit length (Fig. 4), $e_f = K_l F_f/2$ is the combined extension of the springs at failure, and F_f is the force per unit length in the mesh at failure. The stiffness K_l is related to the stiffness K of individual springs through

$$K_l \approx \frac{K}{S} \tag{2}$$

where S is the wire spacing depicted in Fig. 3. Spacing S depends on the dimensions A and B of the mesh (see Fig. 3) as follows

$$S = \frac{A}{\sqrt{1+\dfrac{A^2}{B^2}}} \tag{3}$$

The force in the mesh at failure (per unit length) is given by

$$F_f \approx \frac{F_w}{S} \tag{4}$$

where F_w is the tensile strength of an individual wire, computed as

$$F_w = \frac{\pi}{4}\sigma_y D_w^2 \tag{5}$$

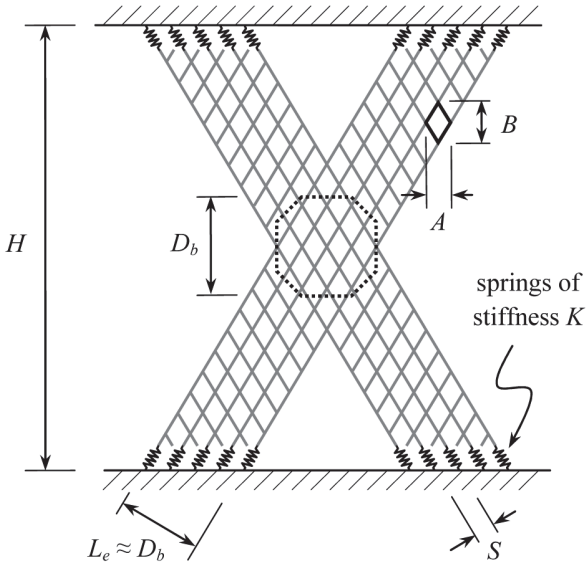

Fig. 3. Cross-shaped region of wire mesh sustaining highest levels of axial stress during block impact.

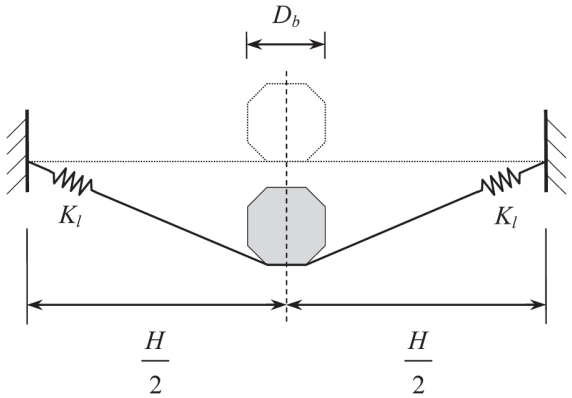

Fig. 4. Schematic of two-dimensional block impact.

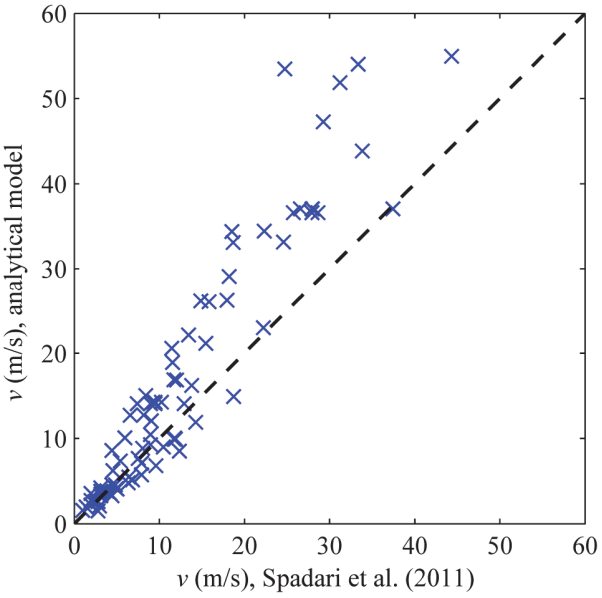

Fig. 5. Comparison of predicted critical velocities from Spadari et al. [15] and analytical model, Eq. (12).

Upon substitution of Eqs. (2)-(5) into Eq. (1), the energy absorbed per unit length of the mesh at failure is

$$E_f = \frac{\pi^2}{16}\frac{\sigma_y^2 D_w^4}{K_l S^2} \tag{6}$$

To account for both strips of mesh in Fig. 3, the total energy absorbed at incipient failure is given by $2E_fL_e = 2E_fD_b$, and balance of energy therefore requires

$$E_k = 2E_f D_b \tag{7}$$

The final expression for the critical energy, obtained by combining Eqs. (6) and (7), is thus

$$E_k = \frac{\pi^2}{8}\frac{\sigma_y^2 D_b D_w^4}{K_l S^2} \tag{8}$$

or, in terms of the stiffness K of individual springs,

$$E_k = \frac{\pi^2}{8}\frac{\sigma_y^2 D_b D_w^4}{KS} \tag{9}$$

To obtain an expression of the critical velocity v, Eq. (8) is combined with the expression of the critical energy

$$E_k = \frac{1}{2}mv^2 \tag{10}$$

where m is the mass of the block. Mass m is related to the nominal diameter D_b and block density ρ through

$$m = c\rho D_b^3 \tag{11}$$

where coefficient c depends on the geometry of the block ($c \approx 0.71$ for the geometry shown in Fig. 2). With the aid of Eqs. (9)-(11), one may solve for the critical velocity v to find

$$v = \frac{\pi}{2\sqrt{c}}\sqrt{\frac{\sigma_y^2 D_w^4}{\rho D_b^2 KS}} \tag{12}$$

From Eq. (9), it can be seen that the critical energy decreases as the block diameter D_b decrease, and the simple model therefore captures the bullet effect. Moreover, the model predicts that the critical energy exhibits linear dependence on the block size. On the other hand, the model predicts that the critical velocity increases as the block size decreases, which also agrees with observations from previous experimental and numerical studies (e.g., [8, 11]). In the next section, predictions from Eqs. (9) and (12) are compared with data from previous works.

4. COMPARISON WITH PREVIOUS STUDIES

Spadari et al. [15] assessed critical velocities for numerous combinations of K, D_b, σ_y, D_w, and A by means of the finite element simulations described in Section 2. In Fig. 5, the critical velocities evaluated numerically are compared with the analytical predictions of Eq. (12). It can be seen that the approximate model predicts critical velocities that are generally larger than those determined from numerical simulation. This result is perhaps somewhat surprising, as one would expect that the disregard for the true three-dimensional deformation of the wire mesh, coupled with neglect of the energy absorbed by the wire mesh, would lead to an underestimation of the energy absorbed by the barrier and a commensurate underestimation of the critical velocity. A likely explanation for this discrepancy is that appreciable stresses are generated in the wire mesh due to bending in the numerical simulations, and these added bending stresses cause the mesh to fail at lower impact energy.

Spadari et al. [15] also synthesized the variables characterizing barrier performance in a scaling relationship involving three dimensionless groups, defined as follows

$$E^* = \frac{\rho v^2 H}{K} \tag{13}$$

$$S^* = \frac{K}{H\sigma_y} \tag{14}$$

$$G^* = \frac{D_w}{D_b^{3/4} A^{1/4}} \tag{15}$$

where H is the dimension of the wire mesh shown in Fig. 3. Their proposed scaling relationship, referred to as the "RoBaP model," was found to have the form

$$E^* = \alpha \left(S^* \right)^{\beta} \tag{16}$$

where α and β depend on G^*. By way of comparison, the prediction from the analytical model, Eq. (12), can be manipulated into a form very similar that of Eq. (16), viz.

$$E^* = \frac{\pi^2}{4c} G' \left(S^* \right)^{-2} \tag{17}$$

where

$$G' = \frac{D_w^4}{D_b^2 HS} \tag{18}$$

It can be seen that the approximate analytical model is in agreement with the RoBaP model (Eq. (16)) provided G^*, the so-called geometric parameter, is redefined as G' (Eq. (18)). Upon introduction of G', the constants in Eq. (16) are given simply as $\alpha = 3.5G'$ and $\beta = -2$ for a block whose geometry is given by $c = 0.71$.

In Fig. 6, predictions based on Eq. (17) are compared with the data obtained in the study by Spadari et al. [15]. Qualitatively, there is very good agreement, with an increase in G' causing an upward shift of the E^*-S^* curve. Quantitatively, there are clear discrepancies between the analytical model and the data from numerical simulations, especially at low values of S^*.

While Spadari et al. [15] fitted curves of the form given by Eq. (16) to their data, the function specifying the exact relationship between E^*, S^*, and G^* was not fully defined. Upon replacing G^* with G', the analytical model presented in this paper points to the specific form given by Eq. (17). If one chooses this same basic form but selects the coefficient and exponent based on least-squares regression, the following can be obtained

$$E^* = 465 G' \left(S^* \right)^{-\frac{3}{2}} \tag{19}$$

The trends from Eq. (19) are compared to the data of Spadari et al. [15] in Fig. 7. Despite some evident scatter, the overall trends in the numerical data are predicted very well by Eq. (19).

It may be noted that the dimension H nowhere appears in the analytical model (Eqs. (9) and (12)), and H can indeed be eliminated from Eq. (17). The absence of H is due to the assumptions of the model, where energy absorbed by the mesh itself is neglected. In contrast, Eq. (19) suggests that the critical velocity and critical energy depend on H. Further refinements to the analytical model, discussed in detail in the concluding remarks, may lead to predictions similar to Eq. (19).

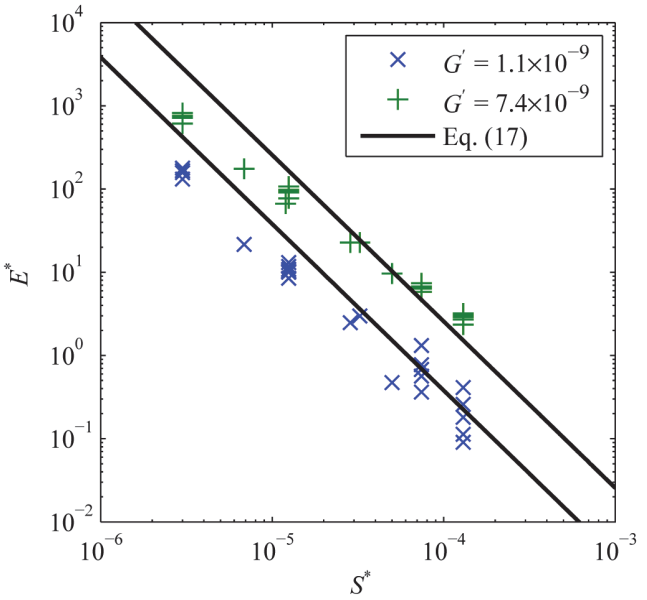

Fig. 6. Relationship between dimensionless groups E^* and S^* for two values of G'. Discrete points represent data from numerical simulations by Spadari et al. [15], and lines show predictions based on approximate analytical model (Eq. (17)).

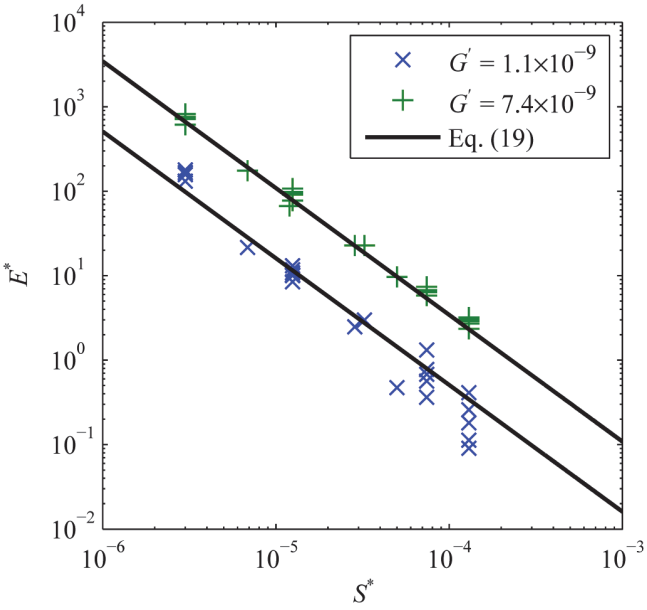

Fig. 7. Prediction of fitted model (Eq. (19)) as compared with data from numerical simulations by Spadari et al. [15].

As a final comparison with data available in the literature, the trends predicted by the analytical model are plotted against critical velocities and critical energies assessed by Cazzani et al. [8] from comprehensive numerical simulations of block impact on a full barrier. A complete quantitative comparison with the data of Cazzani et al. [8] would require determination of a representative value of stiffness K (or K_l) for the barrier modeled in their study. Rather than perform this step (and attempt to identify suitable values for other

parameters), we directly fit curves of the form given by the analytical predictions of Section 3 (Eqs. (8) and (12))

$$v = \frac{a}{D_b} \tag{20}$$

$$E_k = bD_b \tag{21}$$

where coefficients a an b in Eqs. (20) and (21) are evaluated using least-squares regression.

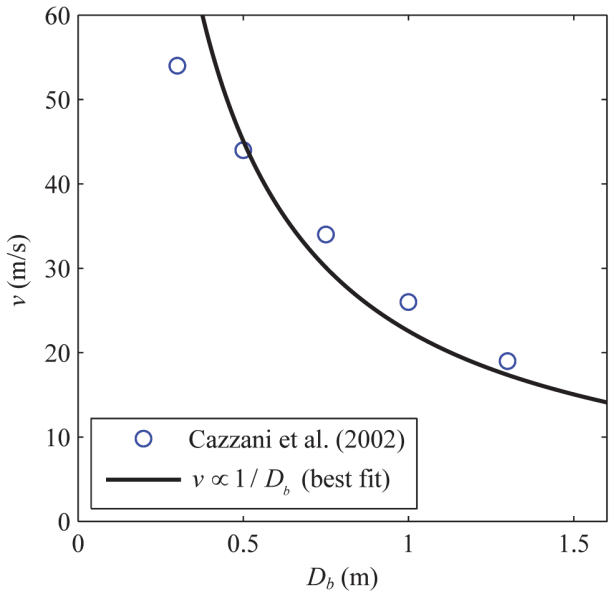

Fig. 8. Critical velocity versus block diameter from Cazzani et al. [8] together with best-fit trend based on approximate analytical model.

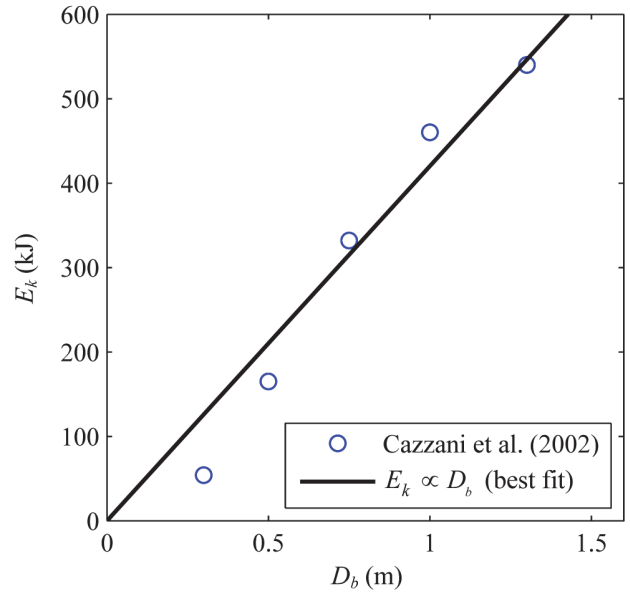

Fig. 9. Critical energy versus block diameter from Cazzani et al. [8] together with together with best-fit trend based on approximate analytical model.

The best-fit curves of Eqs. (20) and (21) are plotted together with the data of Cazzani et al. [8] in Figs. 8 and 9. It is seen that the trends predicted by the approximate analytical model are in good agreement with the data from simulations of a full barrier. On the other hand, deviations are also evident, that these suggest that there is merit in further refining the approximate analytical model.

5. CONCLUDING REMARKS

The paper presents a simple analytical model for predicting perforation of a flexible rockfall protection barrier by normal block impact. This model not only provides physical insight into the impact problem but also predicts the dependencies of critical energy and critical velocity on block size surprisingly well when compared to data from previous studies on barrier impact. Specifically, the model predicts that the critical energy is proportional to the nominal block diameter, whereas critical velocity is inversely proportional to the nominal block diameter. With future refinements, the model promises to furnish quantitatively accurate predictions. These predictions are of potentially great value in engineering practice, as they enable an immediate characterization of the performance of a flexible barrier over a range of block sizes, without resorting to costly physical tests or computationally expensive numerical simulations. To fully validate the findings presented in this paper, well-controlled physical tests aimed at evaluating critical velocities over a range of block sizes are needed.

A number of potential improvements to the analytical model can be identified, and several of these will be developed in a forthcoming paper. In the analysis presented in this paper, the springs supporting the wire mesh absorb all of the impact energy, and greater accuracy would be attained if both elastic and plastic deformations within the mesh were included as sources of energy absorption. Also, the present study adopts a relatively crude criterion for mesh failure. By including the effects of bending, as well as details relating to the local interaction of wires around the impacting block, the model's accuracy will undoubtedly improve. Finally, it may be possible to develop analytical models that consider a fully three-dimensional mode of deformation. Such models would allow for more accurate assessment energy absorption, and they would possibly enable direct incorporation of structural details of the full barrier (e.g., cables and posts).

REFERENCES

1. Smith, D.D. and J.D. Duffy. 1990. *Field tests and evaluation of rockfall restraining nets, final report*. Sacramento: California Department of Transportation.
2. Hearn, G., R.K. Barrett, and H.H. Henson. 1995. Testing and modeling of two rockfall barriers. *Transportation Research Record*, No. 1504, 1-11.
3. Peila, D., S. Pelizza, and F. Sassudelli. 1998. Evaluation of Behaviour of Rockfall Restraining Nets by Full Scale Tests. *Rock Mechanics and Rock Engineering* 31(1): 1-24.
4. Grassl, H., A. Volkwein, E. Anderheggen, and W.J. Ammann. 2002. Steel-net rockfall protection - experimental and numerical simulation. In *Proceedings of the Seventh International Conference on Structures Under Shock and Impact*, eds. N. Jones, C.A. Brebbia, and A.M. Rajendran. Montreal, Canada. 143-153.
5. Bertolo, P., C. Oggeri, and D. Peila. 2009. Full-scale testing of draped nets for rock fall protection. *Canadian Geotechnical Journal* 46(3): 306-317.
6. Arndt, B., T. Ortiz, and A.K. Turner. 2009. Colorado's Full-Scale Field Testing of Rockfall Attenuator Systems. In *Transportation Research Circular*, No. E-C141. Washington, DC: Transportation Research Board.
7. Anderheggen, E., A. Volkwein, and H. Grassl. 2002. Numerical simulation of highly flexible rockfall protection systems. In *Proceedings of the Fifth World Congress on Computational Mechanics* (WCCM V), eds. H.A. Mang, F.G. Rammerstorfer, and J. Eberhardsteiner. Vienna, Austria.
8. Cazzani, A., L. Mongiovì, and T. Frenez. 2002. Dynamic finite element analysis of interceptive devices for falling rocks. *International Journal of Rock Mechanics and Mining Sciences* 39(3): 303-321.
9. Volkwein, A. 2005. Numerical Simulation of Flexible Rockfall Protection Systems. In *Proceedings of the 2005 ASCE International Conference on Computing in Civil Engineering*, eds. L. Soibelman and F. Peña-Mora. Cancun, Mexico.
10. Cantarelli, G., G.P. Giani, G. Gottardi, and L. Govoni. 2008. Modelling Rockfall Protection Fences. In *Proceedings of The First World Landslide Forum*, eds. N. Casagli, R. Fanti, and V. Tofani. Tokyo, Japan. 662-667.
11. Buzzi, O., A. Giacomini, M. Spadari, and S. Fityus. 2011. Numerical modeling of a rock fall mesh perforation upon impact. In *Proceedings of the 13th International Conference of the International Association for Computer Methods and Advances in Geomechanics*, eds. N. Khalili and M. Oeser. Sydney, Australia. 1141-1146.
12. Giani, G.P. 1992. *Rock slope stability analysis*. Rotterdam: Balkema.
13. De Col, R. and S. Cocco. 1996. Motivazioni tecniche ed economiche per la standardizzazione delle prove sulle opere paramassi nella Provincia Autonoma di Trento, In *La protezione contro la caduta massi dai versanti rocciosi*. Torino: Associazione Georisorse e Ambiente. 65-72.
14. Volkwein, A., L. Melis, B. Haller, and R. Pfeifer. 2005. Protection from Landslides and High Speed Rockfall Events: Reconstruction of Chapman's Peak Drive. In *Proceedings of the 2005 IABSE Symposium*. Lisbon, Portugal. 47-54.
15. Spadari, M., A. Giacomini, O. Buzzi, and J.P. Hambleton. 2012. Prediction of the Bullet Effect for Rockfall Barriers: a Scaling Approach. *Rock Mechanics and Rock Engineering* 45(2): 131-144.
16. EOTA. 2008. Guideline for European technical approval of falling rock protection kits. ETAG 27. Brussels: EOTA.